

Modeling the Global Distribution of Plasma Parameters on Coronal Source Surface for Different Solar Phases Using 1AU Observations

Yi Yang,^{1,2} Fang Shen,^{1,*} and Xueshang Feng¹

¹*SIGMA Weather Group, State Key Laboratory of Space Weather, Center for Space Science and Applied Research, Chinese Academy of Sciences, Beijing 100190, China;*

²*College of Earth Sciences, University of Chinese Academy of Sciences, Beijing 100049, China;*

Abstract. In this paper, we have developed an empirical model of the global distribution of plasma parameters on the coronal source surface (at 2.5 solar radii (Rs) in our study) by analyzing observations from Ulysses and OMNI data. We use this model to construct the global map of source surface plasma for four typical Carrington Rotations (CRs) during different phases of solar activity, and analyze the basic characteristics of the distribution. A simple validation of the model is made by comparing the density and velocity distribution with the *pB*-inversed density and Wang-Sheeley-Argge (WSA) model velocity. The preliminary results show that our model gives reasonable large scale distribution of source surface plasma parameters at different phases of solar activity.

1. Introduction

The study of the global distribution of plasma parameters and magnetic field on coronal source surface has great significance in determining the inner-boundary condition of constructing a three-dimensional (3D) heliosphere, and improving the accuracy of 3D MHD models. Some progress on this topic has been made in recent years (Wei et al., 2003; Shen et al., 2010). The most recent statistical and numerical study of the global distribution for the corona plasma and magnetic structure near 2.5Rs made great improvement (Shen et al., 2012; Shen et al., 2013) in deriving the solar wind speed at 1AU, by using the expansion factor f_s and the angular distance θ_b . The expansion factor f_s is defined as $f_s = (B_R/B_\odot)^2(R/R_\odot)^2$ (Wang and Sheeley, 1990), and θ_b refers to the minimum angular separation (at the photosphere) between an open field foot point and its nearest coronal hole boundary (Arge and Pizzo, 2000). They can be used to specify the open field region and the close field region, and separate the high-speed solar wind from the low-speed solar wind (Feng et al., 2010).

Solar wind reaches Earth a few days after leaving the source surface, thus the solar wind parameters near Earth may reflect some basic plasma characteristics on the source surface. In the present paper, we use the plasma distribution characteristics

* Corresponding author: Fang Shen, Email: fshen@spaceweather.ac.cn

obtained from *in-situ* observations near 1AU and the feature of current sheet deduced from potential field source surface (PFSS) model (Altschuler and Newkirk, 1969) to estimate the global distribution on the source surface.

The paper is organized as follows. In Section 2, we describe the procedure to develop our empirical source surface model. In Section 3, global maps of the source surface plasma parameters and magnetic field of four typical CRs during different solar phases are presented and analyzed. Comparison of our density maps with those inverted from polarized brightness (*pB*) observations are made, as well as the comparison of our outflow velocity maps with WSA model. A summary is provided in Section 4.

2. Data and Method

The joint ESA-NASA Ulysses mission has conducted the first-ever survey of the Sun's environment from the equator to the poles at all latitudes. It completed three orbits of the Sun, and the perihelion is about 1.3AU, which is close to the distance from Earth to the Sun. The rapid pole-to-pole (about -80 to 80 degree) passages allow us to obtain the latitudinal variation characteristics of solar wind parameters. The first and third rapid flybys which occurred near solar minimum show very similar large scale distributions, while the second flyby which occurred near solar maxima might conceal the basic large scale characteristics because of large amount of solar transients. We choose the third fast-latitudes scan in 2007/08, because this period is near the solar minimum of 23rd solar cycle and the relatively stable Sun can show its basic character more clearly.

The daily averaged Ulysses data could be downloaded from the Space Physics Data Facility (SPDF) of NASA/Goddard Space Flight Center. Since the actual value of solar wind parameter could change in time but the basic character might be stable, a normalization of the original data is performed to extract the basic latitudinal variation pattern. Then the normalized velocity is fitted by the function: $V(\theta) = p_1 + p_2 e^{-0.5((\theta-p_3)/p_4)^2}$, and the density is fitted by: $\rho(\theta) = 1/(q_1 + q_2\theta + q_3\theta^2)$. The normalized observable and fitting results are shown in Figure 1.

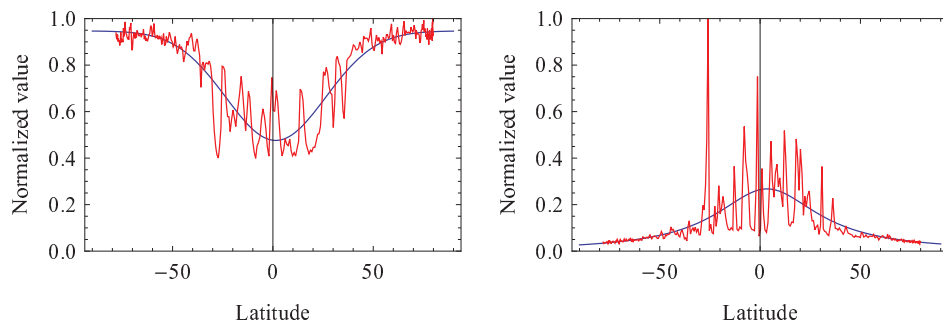


Figure 1. Fitting results of normalized Ulysses data. The red lines refer to normalized observable and the blue ones are curves of fitting function. *Left*: velocity result. *Right*: density result.

We assume the latitude which has the lowest value of fitting velocity or the highest value of fitting density coincides with the latitude of the heliospheric current sheet (HCS). As shown in Figure 1, the bottom or the top of the blue fitting lines locates at the equator. Since the observation period is near solar minimum, the HCS should

also stay near the equatorial plane. Then, we suppose that the highest density or lowest velocity locate near the HCS during all the time, and latitudinal variation feature related to the latitudinal distance to HCS remains the same with the Ulysses fast-latitudes scan which we have fitted above. Therefore, we can try to obtain the latitudinal distribution of density and velocity for all solar active phases instead of just solar minimum with this assumption.

Potential Field Source Surface (PFSS) model (Altschuler and Newkirk, 1969) is used to calculate the corona magnetic field and give the HCS position on the source surface. Line-of-sight (los) photospheric field measurements from Wilcox Solar Observatory (WSO) are used as input of the PFSS model. The data could be downloaded from <http://wso.stanford.edu/synsourcel.html>.

For an arbitrary point P on the source surface, it has a latitude θ , and a corresponding $|\theta - \theta_{HCS}|$ which refers to the latitudinal distance from P to the HCS, as shown in Figure 2. By replacing the θ with $|\theta - \theta_{HCS}|$ in the fitting function presented above, we could deduce the latitudinal distribution function for all solar phases.

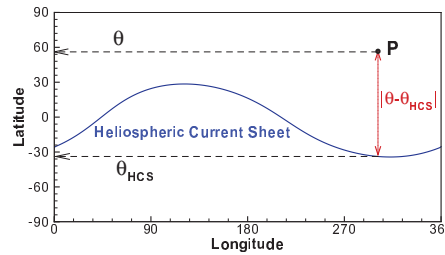


Figure 2. Schematic diagram for the latitudinal distance from P to HCS.

OMNI data set is primarily a 1963-to-current compilation of near-Earth solar wind magnetic field and plasma data from several spacecraft in geocentric or L1 (Lagrange point) orbits. The hourly-averaged plasma data of separate Carrington Rotations (CRs) could be extracted from NASA/GSFC's OMNI data set through OMNIWeb. The OMNI data can provide the longitudinal variation of solar wind parameters at about 1AU near Earth. Considering the OMNI data set provides ecliptic observations only, it is just used to limit the distribution near ecliptic regions (± 15 degree in this paper).

Assuming the solar wind speed is constant between the source surface and Earth, we can map back the 1AU-observed solar wind parameters to the source surface along Parker spiral (Parker et al, 1958). The mapping process uses the function $\phi = \phi_e + \omega t = \phi_e + \omega(215Rs - 2.5Rs)/v$, where ϕ_e is the Carrington Longitude of the observer near Earth, ϕ is the corresponding Carrington Longitude at source surface, ω is the angular speed of the Sun's rotation (corresponding to a period of 26.2 days), and t is the time that solar wind propagate from source surface (2.5Rs) to Earth (215Rs).

Similar to the Ulysses process, normalization and fitting of the OMNI data for separate CRs are performed to obtain the longitudinal characteristics. The normalized OMNI velocity and density are both fitted by the function $f(\phi) = \sum_1^n (a_n \phi^\gamma)$, where ϕ is the Carrington Longitude at source surface, $\gamma = 0, \frac{1}{2}, 1, \frac{3}{2}, 2, \frac{5}{2}, 3, \dots$, and $f(\phi)$ can be $V(\phi)$ or $\rho(\phi)$. The fitting results of OMNI data for CR2013 are presented as an example in Figure 3.

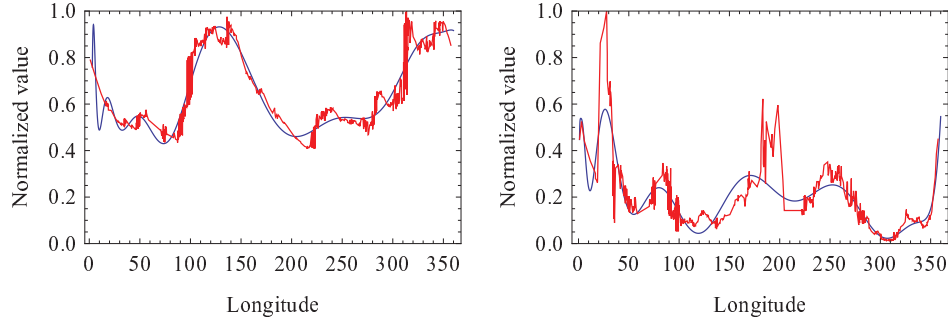


Figure 3. Example of fitting results of the normalized OMNI data (CR2013). The red lines are normalized observable and blue ones are fitting curves. *Left*: velocity result. *Right*: density result.

After the fitting and mapping procedure, we can finally construct latitude-longitude maps to estimate the global distribution of density and velocity at the source surface, by using the functions:

$$\rho(\theta, \phi) = \rho_t \rho(|\theta - \theta_{HCS}|) \rho(\phi)$$

$$V(\theta, \phi) = V_t V(|\theta - \theta_{HCS}|) V(\phi)$$

, where ρ_t is the typical density value of current sheet region at 2.5Rs, and V_t is the typical value of high-speed solar wind velocity at the source surface. In this work, we simply assume $\rho_t = 10^6/cm^3$, $V_t = 300km/s$ for all solar phases.

3. Results

In this section, we present the modeling results of global distribution maps of source surface magnetic field and plasma parameters of four typical CRs during different active phases of the 23rd solar cycle, and compare the results with those from other methods.

The global distributions of radial magnetic field, density and velocity at 2.5Rs during different phases of the 23rd solar cycle are shown as latitude-longitude maps in Figure 4. We choose four typical CRs to study the source surface condition for different solar phases, shown as (a)-(d) in Figure 4 respectively. The results show that our model can always describe the basic distribution feature of plasma parameters, although the position of HCS changes during different solar phases.

Figure 5 presents the comparison of results from our model and other method. The first two rows of Figure 5 show the density distribution obtained from polarize brightness (pB) inversion (Van de Hulst et al, 1950) and our model for the four typical CRs. The last two rows of Figure 5 show the radial speed results from our model and WSA model.

The pB data we use are obtained from STEREO/COR1 and SOHO/LASCO white light observation. In the density inversion process, we use IDL routines from SolarSoftWare (SSW) to calculate the field-of-view density map, and then extract the density at 2.5Rs to construct the latitude-longitude maps. It can be seen that our model gives the density distribution of different solar phases very similar to the pB -inversed ones, except the solar maximum. The discrepancy for solar maximum may due to the high solar activity, which causes more solar transients such as flares and CMEs.

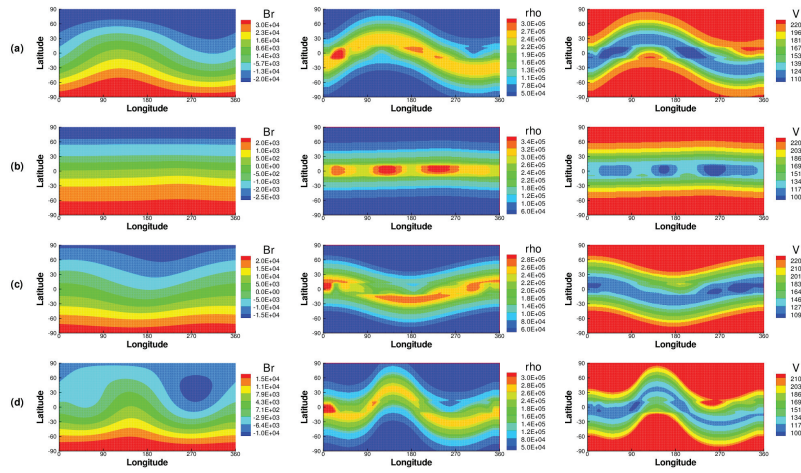


Figure 4. Global distribution of radial magnetic field, density and velocity at 2.5Rs during different phases. (a) CR2013 in 2004 (descending phase); (b) CR2088 in 1993 (minimum); (c) CR2105 in 2010 (ascending phase); and (d) CR2121 in 2012 (maximum).

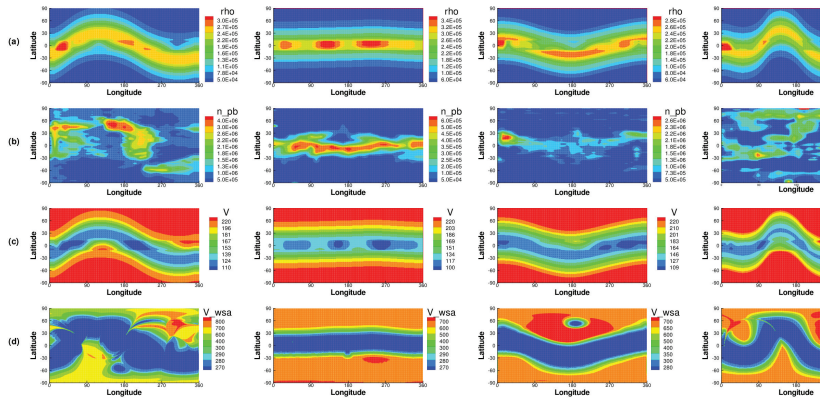


Figure 5. Comparison of density and velocity distribution obtained from our model and other method. (a) density from our model; (b) density from pB inversion; (c) velocity from our model; (d) velocity from WSA model.

The speed from the WSA is specified by $V_{wsa} = 265 + (1.5/(1 + f_s)^{2/7})(5.8 - 1.6e^{[1-(\theta_b/7.5)^3]^{3.5}}$, with the use of expansion factor f_s and minimum angular distance θ_b (Owens et al. 2005). The comparison with WSA model in Figure 5 shows that our approach could approximately give the large scale velocity distributions, because it could present reasonable latitudinal extent of fast and slow wind similar to the WSA. However, the predicted speed values of the two method has considerable differences. It is obvious that the speed from our model is smaller than the result from WSA. One clear reason is that the typical value of high-speed solar wind in our distribution function is much smaller than the high-speed prediction from WSA. Another reason is that the WSA function we use above provides the speed at about 5Rs instead of 2.5Rs, thus some acceleration may happen in this distance. MHD model can also present a rel-

atively low speed than WSA, because the f_s obtained from the steady-state magnetic fields of the MHD model is bigger than the WSA model and will have a large expansion magnetic field and then present a relatively low speed (Feng et al., 2014).

4. Summary

In this study, we have modeled the global distributions of density and velocity on the source surface by deriving distribution functions from Ulysses and OMNI observations. Modeling results of four typical CRs during different phases of the 23rd solar cycle are presented, and have been compared with pB-inversed density and the WSA velocity. The results show that our model could qualitatively represent the large scale characteristics of density and velocity distributions on the source surface.

Further, we intend to use these distributions to obtain the coronal mass outputs flux (F_m) at the source surface, then use the distribution of magnetic field, density and F_m as inputs of a self-consistent MHD method (Shen et al., 2010, 2012) to numerically generate a solar cycle dependent, self-consistent initial inner-boundary for the 3D MHD simulation from near the Sun to Earth.

Acknowledgments. We acknowledge use of NASA/GSFC's Space Physics Data Facility's OMNIWeb service, the daily averaged Ulysses data and hourly averaged low resolution OMNI data are both obtained from the GSFC/SPDF OMNIWeb interface at <http://omniweb.gsfc.nasa.gov>. It should be also acknowledged that the white light brightness data are obtained from STEREO-COR1 and LASCO-C2, solar photospheric magnetic field data are taken from Wilcox Solar Observatory (WSO). This work is jointly supported by the National Basic Research Program of China under Grant No 2012CB825601, the Knowledge Innovation Program of the Chinese Academy of Sciences (KZZD-EW-01-4), the National Natural Science Foundation of China (41174150, 41174152, 41374188, 41474152), and the Specialized Research Fund for State Key Laboratories.

References

- Altschuler, M. D., Newkirk, G. 1969, *Solar Phys.*, 9, 131
 Arge, C. N., Pizzo, V. J. 2000, *J. Geophys. Res.*, 105(A5),10465
 Feng, X., Yang, L. P., Xiang, C. Q., et al. 2010, *Astrophys. J.*, 723, 300
 Feng, X., Zhang, M., Zhou, Y. 2014, *Astrophys. J. Suppl.*, 214(1), 6
 Shen, F., Feng, X., Xiang, C. Song, W. B. 2010, *J. Atmospheric and Solar-Terrestrial Physics*, 72(13), 1008
 Shen, F., Feng X., Xiang C. 2012, *J. Atmospheric and Solar-Terrestrial Physics*, 77, 125
 Shen, F., Feng X., Xiang C., Wu, S. T. 2013, in *ASP Conf. Ser. 474, Numerical Modeling of Space Plasma Flows: ASTRONUM-2012*, 172 (San Francisco: ASP)
 Owens, M. J., Arge, C. N., Spence, H. E., Pembroke, A. 2005, *J. Geophys. Res.*, 110, A12105
 Parker, E. N. 1958, *Astrophys. J.*, 128, 664
 Van de Hulst, H. C. 1950, *Bull. Astron. Inst. Neth.*, 11, 135
 Wang, Y. M., Sheeley Jr., N.R. 1990, *Astrophys. J.*, 355, 726
 Wei, F. S., Feng, X. S., Cai, H. C., Zhou, Q. J. 2003, *J. Geophys. Res.*, 108(A6), 1238